Volume 3
Number 21
7 November 2021
Pages 5971–6244

Nanoscale Advances

rsc.li/nanoscale-advances

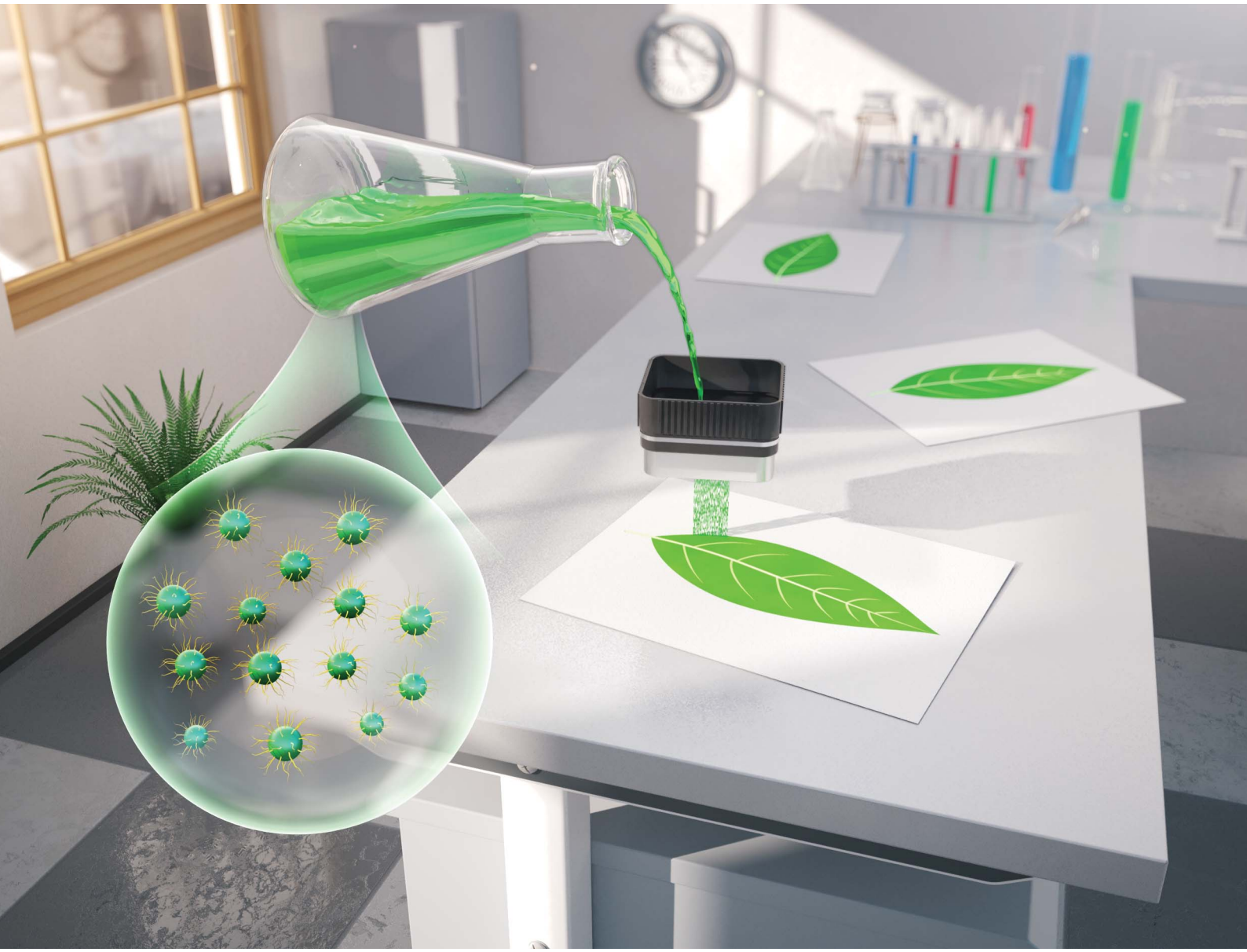

ISSN 2516-0230

ROYAL SOCIETY OF CHEMISTRY

PAPER

Shen Zhou, Mei Zu *et al.*

One-step preparation of Cr_2O_3-based inks with long-term dispersion stability for inkjet applications

NCNST

Nanoscale Advances

ROYAL SOCIETY OF CHEMISTRY

PAPER

View Article Online
View Journal | View Issue

Cite this: *Nanoscale Adv.*, 2021, **3**, 6048

One-step preparation of Cr_2O_3-based inks with long-term dispersion stability for inkjet applications†

Dongjin Xie,[a] Qiuyi Luo,[ab] Shen Zhou, *[ac] Mei Zu*[a] and Haifeng Cheng[a]

Inkjet printing of functional materials has shown a wide range of applications in advertising, OLED display, printed electronics and other specialized utilities that require high-precision, mask-free, direct-writing deposition techniques. Nevertheless, the sedimentation risk of the refractory functional materials dispensed in inks hinders their further implementation. Herein, we present a bottom-up ink preparation strategy based on Cr_2O_3 by a one-step solvothermal method. The obtained ink remained stable under an equivalent natural sediment test for 2.5 years. The chemical composition of the solvothermal product was characterized, and the mechanism of the superior dispersion stability of Cr_2O_3 particles was analysed. These amorphous Cr_2O_3 particles were capped by ligands generated *via* low-temperature solvothermal reactions. Ethanol and acetylacetone covering the particle surfaces play an essential role in enhancing the solubility of Cr_2O_3 particles in the solvent forming the ultrastable colloidal ink. Moreover, this ink was successfully printed using a direct-write inkjet system JetLab®II on nylon fabrics, and the printed area of the fabrics shows a spectral correlation coefficient of 0.9043 to green leaves. Finally, we believe that the one-step bottom-up fabrication method of Cr_2O_3-based pigment inks may provide a general approach for preparing metal oxide-based pigment inks with long-term dispersion stability.

Received 31st March 2021
Accepted 28th July 2021

DOI: 10.1039/d1na00244a

rsc.li/nanoscale-advances

Introduction

Inks based on functional materials (metal oxides, for example) have extended the application of printing techniques from information transferring and colour reproduction to other emerging technologies such as biotechnology and electronics.[1–4] Nowadays, there are several available printing techniques such as inkjet printing,[5] screen printing,[6,7] flexographic and gravure printing[8–10] to deposit functional inks onto substrates. Among them, inkjet printing with a drop-on-demand system has gained extensive interest due to its special features such as direct (masks-free) patterning, noncontact deposition and the minimal waste of materials.[11–14] However, inkjet printing technique has strict requirements for ink properties including particle diameter and rheological parameters. As the nozzle sizes of print head are generally tens of microns,[15] to avoid clogging the nozzle, the functional materials dispersed in ink must be processed into submicron scale, and remain stable during the printing procedure.[16–18]

Chromium oxide (Cr_2O_3) is a high-performance refractory inorganic material with excellent stability and pronounced optical properties. Cr_2O_3 crystallizes in corundum structures at 400 °C, and has a high melting temperature of about 2300 °C. The high-temperature oxidation resistance, chemical inertness and mechanical strength of Cr_2O_3 make it a suitable material for wear and corrosion resistance materials.[19] Moreover, Cr_2O_3 as a green pigment with outstanding tinting strength and migration resistance has been commercialized as C.I. Pigment Green 17 (PG17), and the $3d_3$ electronic configuration of chromium ions endows Cr_2O_3 with chlorophyll-like absorption in the visible (VIS) region.[20–22] This makes Cr_2O_3 a proper pigment for simulating the solar spectrum reflection characteristic of green leaves for camouflage purpose.[23] Since Cr_2O_3 coatings exhibit high reflectance in the whole near-infrared (NIR) region that carry 51% of solar energy, it has the potential to be utilized as coloured radiative coolers, which can reduce solar heating and improve appearance simultaneously.[24,25]

Applying the inkjet printing technology with Cr_2O_3 as the pigment can significantly simplify the process from designing to coating a new camouflage pattern and reduce the cost. Unfortunately, to the best of our knowledge, inkjet printing of Cr_2O_3 has not been reported yet, because ink based on metal oxide particles always suffers from poor dispersion stability and

[a]*Science and Technology on Advanced Ceramic Fibers and Composites Laboratory, College of Aerospace Science and Engineering, National University of Defense Technology, Changsha 410073, China. E-mail: zhoushen@nudt.edu.cn*

[b]*People's Liberation Army of China Unit 95538, Chengdu, 611430, China*

[c]*School of Chemistry and Chemical Engineering, South China University of Technology, Guangzhou 510640, China*

† Electronic supplementary information (ESI) available. See DOI: 10.1039/d1na00244a

tends to agglomerate and precipitate, resulting in clogging in the nozzle while printing.[26]

In a typical procedure of pigment ink preparation, pigments are ground to nanoscale and dispersed into solvents using auxiliaries such as resin and dispersant (top-down approach). Unfortunately, for many pigments such as titanium oxide prepared by this process, their suspensions are dynamically unstable and easy to precipitate, even when using a dispersant. The instability and risk of sedimentation are mainly caused by that the solid pigment particles are artificially dispersed in the system instead of *in situ* generation. To overcome this problem, we propose bottom-up approaches to prepare pigment inks. Bottom-up formation of pigment particles in the liquid phase involves *in situ* nucleation and growth procedure. After nucleation, the newly generated small particles are suspended in the liquid until the particles grow large enough to precipitate and agglomerate to a lower surface energy. By controlling the growth reaction, precipitation of the particles can be prevented, which makes it possible for the *in situ* preparation of particle suspension in one step.

In this work, we present a one-step preparation strategy of chromium oxide-based ink with long-term dispersion stability (2.5 year). Chromium oxide-based pigment powder and dispersion were prepared by a facile solvothermal method. With the decrease in solvothermal temperature down to 200 °C, the final products transform from precipitated powder into colloidal suspension. Multiple characterizations were applied to explore the chemical composition, and possible mechanisms are discussed. It is indicated that acetylacetone generated from the solvothermal reaction plays a significant role in the stabilization of the colloidal suspension. We compared the instability index of our ink based on the as-prepared suspension with a typical ink formulation prepared by a conventional top-down approach (ball-milling) through the space and time-resolved measurement. Moreover, the synthetic ink retains all of the optical advantages that are provided by pristine Cr_2O_3. We demonstrated an ink-jet application for simulating the solar reflection spectrum of natural green leaves. The solar reflection spectral correlation coefficient between the pattern printed on polyethylene terephthalate (PET) films and natural leaves is up to 0.9043. This one-step ink preparation strategy holds great potential for an efficient fabrication process of chromium green patterns with similar solar reflectance to green leaves.

Results and discussion

In order to simplify the steps of Cr_2O_3 preparation, trivalent chromium precursors such as chromium(III) acetylacetone ($Cr(acac)_3$), chromium nitrate, and chromium chloride are preferred in our solvothermal synthesis. Because the trivalent chromium ion is easily hydrolysed in the presence of water, forming undesired chromium hydroxide ($Cr(OH)_3$) that tends to aggregate into heterogeneous loose structures with a large size,[27] $Cr(acac)_3$ with low hygroscopicity and good solubility in alcohol was chosen as the precursor of our solvothermal method.[28] The optical image of samples prepared at different solvothermal temperatures ranging from 180 to 220 °C with 10 °C interval is illustrated in the inset of Fig. 1(a), and each sample shows a different appearance. The sample prepared at 220 °C has a sediment of green powder with a yield of ~95%, which contains all of the chromium element and a colourless supernatant. By contrast, the supernatant of the sample prepared at 210 °C shows a light green colour, indicating an incomplete precipitation of chromium elements at this temperature. Further decreasing the solvothermal temperature to or below 200 °C results in a macroscopic homogeneous colloid with a deeper green colour, and no sedimentation can be observed. These colloids remain stable after either centrifugation or concentration. Salting out the colloid with 1 M NaCl aqueous solution, spherical particles with an average size of 1.75 μm were obtained at 220 °C (SEM image shown in Fig. S1†). Smaller spherical particles were obtained at a lower temperature. However, the particle size distribution illustrated by the SEM image of the salting out sample cannot represent the situation in untreated colloids due to agglomeration in salting-out treatment. To characterize the particle size distribution of our colloids, the laser diffraction method was performed, and the results are listed in Fig. S2 and Table S1.† It shows that two homogeneous colloids have a significant ratio of particles below 100 nm, while this cannot be observed in samples prepared at temperatures above 200 °C, which have micron-scale particle size increasing with the temperature.

To understand the mechanism of the solubility of the pigment particles, UV-Vis absorption spectroscopy was performed. It can be concluded that the solubility is enhanced by acetylacetone, which is generated under low-temperature solvothermal conditions. As shown in Fig. 1(a), with the decrease in temperature, the total absorbance in the range of 200 to 400 nm is significantly intensified. Among these absorption peaks, the shoulder peaks around 273 nm are referred to the concentration of acetylacetone according to absorption peak of acetylacetone at the same wavelength in the reference sample. On the one hand, the absorbance of acetylacetone decreased with the increase in solvothermal temperature, and the two precipitated samples show little absorbance of acetylacetone. On the other hand, addition of acetylacetone into samples prepared at higher solvothermal temperatures makes the sediments dissolve back into the system, which double confirms that acetylacetone plays a vital role in solubility enhancement. It is noteworthy that bare Cr_2O_3 cannot dissolve into ethanol with the addition of acetylacetone. As depicted in Fig. 1(b), removing acetylacetone by heat leads to agglomeration and sedimentation of pigment particles. Adding acetylacetone or lowering the solvothermal temperature to keep acetylacetone, which may cap on the particle surface to prevent aggregation and control growth, results in the formation of a stable colloidal suspension.[29] In addition, the 1–10 μm signal in the bimodal size distribution of the colloids (Fig. S2†) is due to the agglomeration in the circulatory system in which the sample is dispersed into a large amount of ethanol inducing a serious drop of acetylacetone concentration. This is proved by the SEM (Fig. S1†) of the salted-out product prepared at 190 °C, in which no particle bigger than 1 μm is observed, even the particles were agglomerated when being salted out. This signal was removed by using

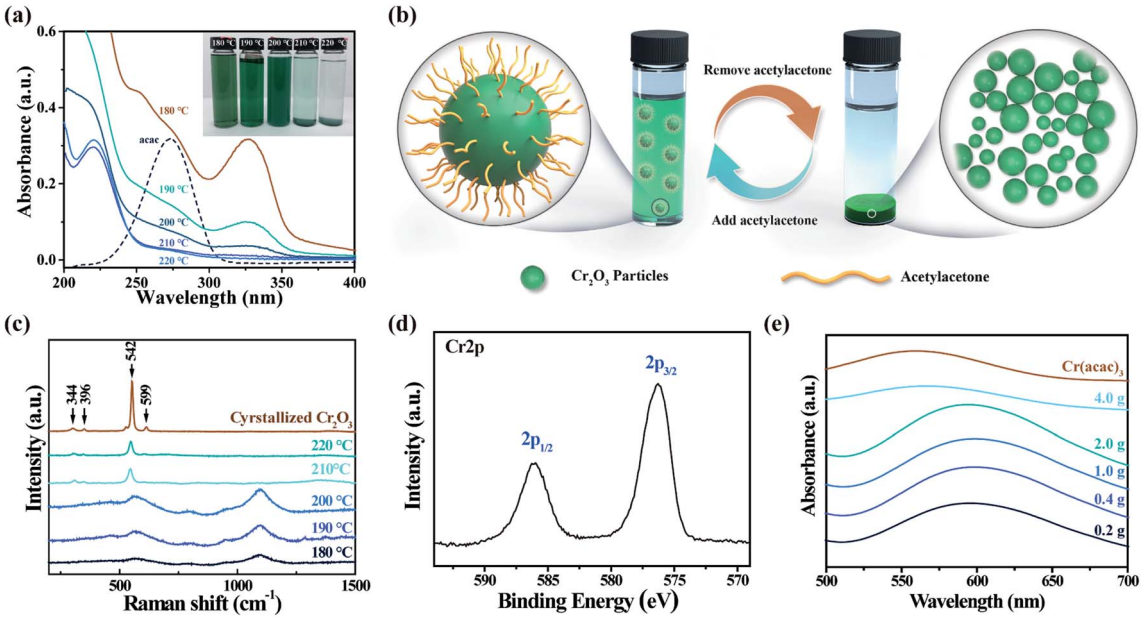

Fig. 1 (a) UV-Vis absorption spectra of the obtained supernatant by a solvothermal method at 180 °C, 190 °C, 200 °C, 210 °C, and 220 °C and acetylacetone in ethanol as the reference. The inset shows the optical image of the aforementioned samples. (b) Schematic of the colloidal suspension to precipitated powder transformation. (c) Raman spectra of the sample obtained by a solvothermal method at 180 °C, 190 °C, 210 °C, 200 °C, and 220 °C and commercial Cr_2O_3 as the reference. (d) X-ray photoelectron spectroscopy (XPS) spectrum of pigment powder obtained by a solvothermal method at 190 °C. (e) UV-Vis absorption spectra of the colloidal product with gradually increasing amounts of chromium sources.

1% v/v acetylacetone ethanol solution in the circulatory system, and the average particle size of 190 °C product is 0.019 μm (Table S1†).

In previous works,[24,30] crystallized Cr_2O_3 can be obtained by annealing the solvothermal product above 400 °C. This method yields a solid-state Cr_2O_3 powder that requires extra steps such as dispersion and filtration to fabricate inks. Annealing is unnecessary in our one-step ink fabrication, and we characterized the as-prepared chemical composition as follows: in Fig. 1(c), the Raman spectra of the colloids (180 °C, 190 °C, and 200 °C) and powder (220 °C) without the annealing process compared with crystallized Cr_2O_3 are demonstrated. The peak positions of crystallized Cr_2O_3 and the as-prepared powder at 344 (E_g), 396 (E_g), 599 (E_g) and 542(A_{1g}) cm^{-1} are in agreement with bulk Cr_2O_3.[31] The spectra of colloids prepared at lower temperatures exhibit a broaden Raman peak of A_{1g} mode at 564 cm^{-1} with a slightly blue shift; besides, a strong peak and a very weak peak that appear at 1095 cm^{-1} and 893 cm^{-1} were assigned to the C–O stretching and C–C stretching modes of the ethanol solvent and organic byproduct;[32] moreover, no Raman shift can be observed at 530 cm^{-1} and 850 cm^{-1}, attributed to Cr–O–H bending and stretching modes of $Cr(OH)_3$.[33] This suggests that the hydrolysis process yielding $Cr(OH)_3$ is avoided by using $Cr(acac)_3$ as the precursor. To double confirm the chemistry of the as-prepared sample, X-ray photoelectron spectroscopy (XPS) was performed, shown in Fig. 1(d), and details of the XPS result are listed in Table S2.† The Cr 2p spectrum of the sample prepared at 190 °C shows two main peaks at 576.6 and 586.4 eV, which were respectively assigned to Cr $2p_{3/2}$ and Cr $2p_{1/2}$. Referring to Biesinger, *et al.*, the peak value and FWHM of Cr 2p and O 1s are more similar to those of Cr_2O_3 than $Cr(OH)_3$.[34] From these results, we can deduce that Cr_2O_3 without $Cr(OH)_3$ impurities was obtained by a solvothermal reaction at different temperatures.

Generally, the mass ratio of the pigment in inkjet inks is 5–10%; while that of our colloids is only up to 0.02%. To elevate the throughput of our method, the addition of $Cr(acac)_3$ is gradually increased from 0.2 to 4.0 g in a 100 mL Teflon-lining autoclave. Fig. 1(e) displays the UV-Vis absorption spectra of the solvothermal product obtained with the addition of different amounts of $Cr(acac)_3$ at 190 °C. While the optical properties of the synthetic ink obtained with reagents considerably exceeding the saturation limit at room temperature were similar, a significant change is observed when the addition is increased to 4.0 g. This changed spectrum shows a similar absorption to $Cr(acac)_3$ at 580 nm and no $4A_{2g}$ to $4T_{2g}$ absorption of Cr_2O_3 at 610 nm.[35] It proves that the solvothermal reaction can tolerant a maximum addition of $Cr(acac)_3$ up to 2.0 g due to the enhancement of solubility and reactivity at high temperatures and pressures of solvothermal conditions, but the reaction will not be effectively conducted when the addition of $Cr(acac)_3$ reaches 4.0 g.

As mentioned above, acetylacetone act as a capping ligand to enhance the solubility of Cr_2O_3 particles in ethanol. The mass ratio and thermal stability of the ligand are revealed by thermogravimetric analysis (TGA) of the dried sample. In Fig. 2(a), a two-step weight loss process is found in atmosphere with the temperature increasing from 20 to 1000 °C at a rate of

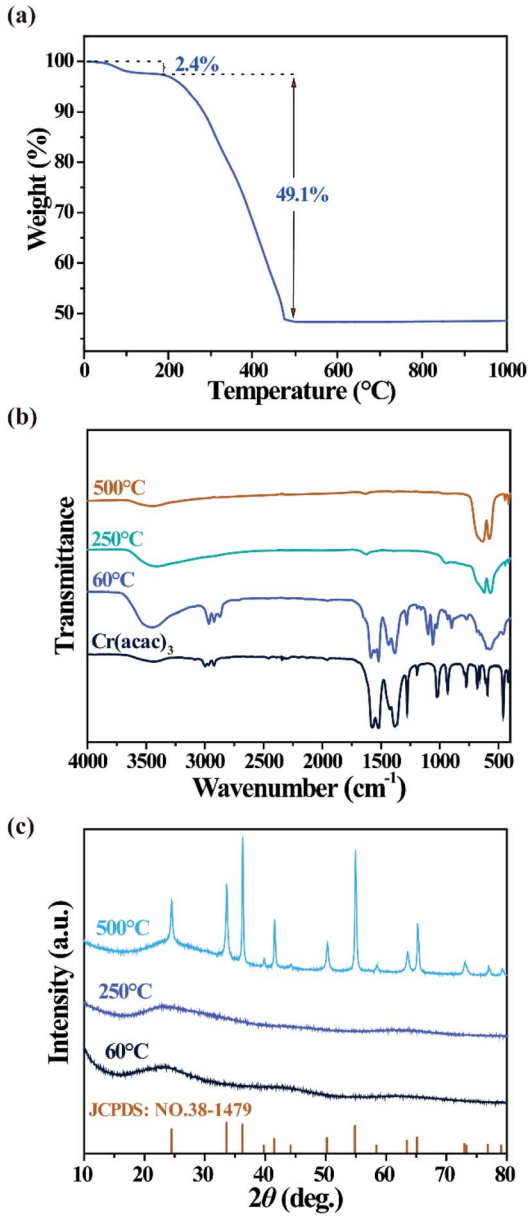

Fig. 2 (a) Thermogravimetric analysis (TGA) of colloidal Cr_2O_3 particles salting out *via* a NaCl aqueous solution. (b) Fourier-transform infrared (FTIR) transmittance of colloidal Cr_2O_3 particles annealed at 60 °C, 250 °C, and 500 °C and $Cr(acac)_3$ as the reference. (c) X-ray diffraction (XRD) patterns of colloidal Cr_2O_3 particles annealed at 60 °C, 250 °C, and 500 °C and JCPDS file no. 38-1479 (drop lines).

5 °C min^{-1}. The first minor weight loss of 2.4% is caused by the desorption of solvent molecules. The main weight loss at 200–460 °C is assumed to be due to the decomposition of the organic moiety. To further confirm our assumption, the sample was treated at 60, 250, and 500 °C for 2 h, and their Fourier-transform infrared (FTIR) transmittance spectra are illustrated in Fig. 2(b). After annealing at 250 or 500 °C, the sample exhibits four absorption peaks at 414, 445, 579 and 635 cm^{-1}, which were assigned to the inter-atomic vibration mode of commercial Cr_2O_3.[36] However, the sample dried at 60 °C shows not only absorption of commercial Cr_2O_3, but also similar absorption peaks to $Cr(acac)_3$, including C=O stretching (1576 cm^{-1}), C=C + νC=O stretching (1526 cm^{-1}), C–H bending (1320-1470 cm^{-1}), and C–C + C–O stretching (1281 cm^{-1}). Besides, two extra peaks located at 1059 cm^{-1} and 1099 cm^{-1} were assigned to C–O stretching, and this C–O bond can only come from ethanol.[32] Moreover, the strength of the wide absorption band at 3459 cm^{-1} indicates the amount of absorbed water of each sample. Therefore, it is revealed that, besides Cr_2O_3, the solvothermal product is composed of acetylacetone, ethanol and absorbed water, which can be eliminated at temperatures above 250 °C. The X-ray diffraction (XRD) patterns are displayed in Fig. 2(d). All XRD peaks of the sample annealed at 500 °C can be indexed to Cr_2O_3 (JCPDS card # 85-0869), while upon annealing at lower temperatures, amorphous Cr_2O_3 was obtained instead of crystalline Cr_2O_3. Accordingly, amorphous Cr_2O_3 capped by acetylacetone and ethanol is the chemical composition of the as-prepared colloidal particles.

As-prepared colloids were concentrated by rotary evaporation, and diethylene glycol diethyl ether was added to adjust the viscosity and surface tension to 5 mPa s and 25.8 mN m^{-1} suitable for ink printing, thus the chromium oxide-based colloidal ink was obtained. The whole fabrication process of this ink is a single bottom-up solvothermal method followed by a simple adjustment of the rheological parameter, which can be considered as a one-step process.

The dispersion stability of the colloidal ink compared with the conventional top-down ball-milled ink is demonstrated by an analytical centrifuge technology, which allows instant measurement of the transmittance of light in different positions of cuvettes as a function of time.[37,38] The data are displayed as a function of the radial position, as distance from the center of the rotation. The progression of the transmission profiles contains the information on the kinetics of the sediment process.[39] Fig. 3(a) shows the series of transmission *vs.* position profiles obtained for top-down ink at 4000 rpm with 30 s recording interval for 5 h to simulate an equivalent natural sedimentation for 2.5 years. Throughout the sedimentation process, the air–liquid boundary remains at the radial position, 107 mm from the center of centrifugation. The first profile exhibits a low transmittance (approx. 2%) and shows no liquid–solid boundary. With the centrifugal force applied to the top-down ink, the transmittance close to the center is gradually increasing up to 90%; the liquid–solid boundary moves simultaneously from the left to the right, and stabilizes at 128 mm till the last profile, indicating a complete sedimentation process from the homogeneous phase to the separated phase. The optical images of inks after centrifugation are illustrated in Fig. 3(b), and the SEM image of the ball-milled Cr_2O_3 particles is shown in Fig. S4(d).† In contrast, the profiles of our colloidal ink in Fig. 3(c) are constant during the characterization. The higher transmittance profiles were recorded using a solvothermal product at 190 °C in Fig. S3,† which is similar to the ink, except that the air-liquid boundary is right shifted due to the evaporation of ethanol and a slightly overall decrease in transmittance due to the increase in the concentration. From these results, it can be observed that our colloidal ink is promising to avoid sedimentation and maintain its homogeneity for at least

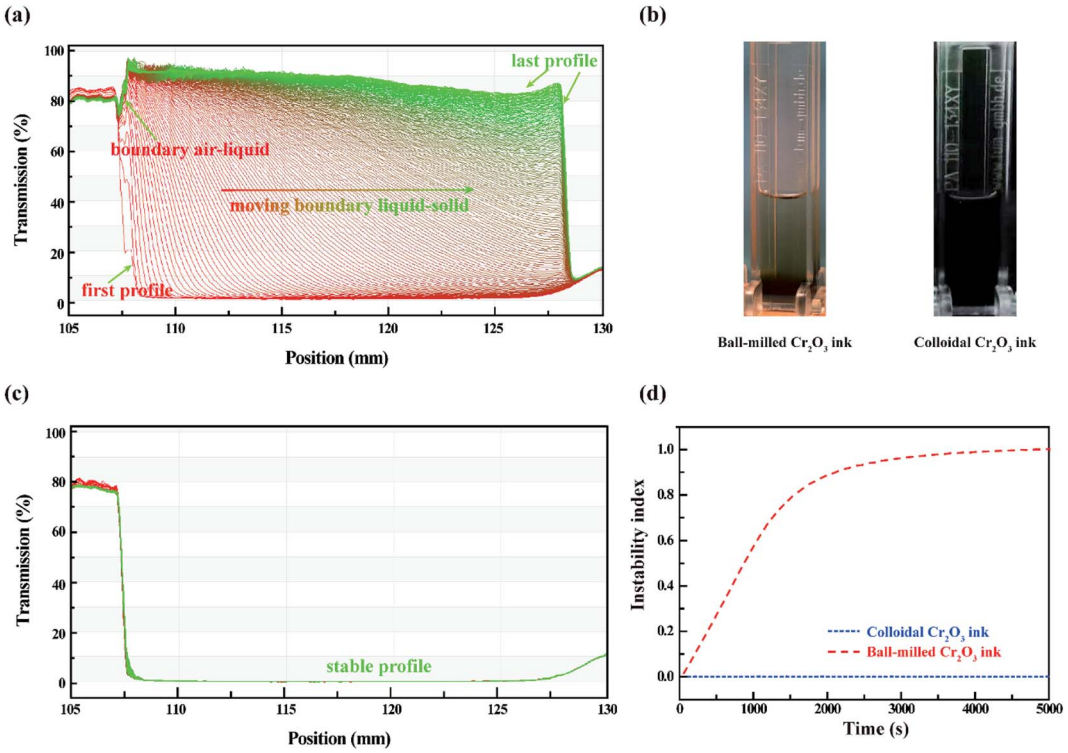

Fig. 3 Transmission *vs.* position profiles of (a) ball-milled Cr_2O_3 ink and (c) colloidal Cr_2O_3 ink, obtained using a dispersion analyser LUMi-Sizer® at a centrifugation speed of 4000 rpm. (b) Optical images of the ball-milled Cr_2O_3 ink (left) and our colloidal Cr_2O_3 ink (right) after centrifugation. (d) Instability of the ball-milled Cr_2O_3 ink (red dash line) and colloidal Cr_2O_3 ink (blue dot line), obtained using a dispersion analyser LUMi-Sizer® at a centrifugation speed of 4000 rpm.

2.5 years. In Fig. 3(d), the 'instability index' of both samples was calculated using the delivered software (SepView 6.0; LUM, Berlin, Germany). The value of the index is a dimensionless number between 0 (very stable) and 1 (very unstable).[40] The mathematical detail is given by Detloff *et al.*[41] The instability index of the top-down ink is approximately 1, at the time of 4000 s, and the sedimentation of the Cr_2O_3 particles is over. The equivalent natural duration is approximate 100 days. However, the colloidal ink possesses an instability index of 0 during the 2.5 year simulation.

A direct-write inkjet system JetLab®II (MicroFab Technologies) was used to deposit the Cr_2O_3 colloidal ink onto nylon fabrics. In Fig. 4(a), the ink fabrication and inkjet printing application are schematically depicted: printable colloidal ink was obtained by solvothermal treatment of $Cr(acac)_3$ followed by concentration to adjust its rheological parameter and the mass ratio of the pigment. This ink can be patterned on fabrics *via* inkjet printing technology. The morphology of the patterned area was characterized by SEM, as shown in Fig. 4(b). As can be observed, polydisperse Cr_2O_3 particles are uniformly distributed on the polyurethane layer of the fabrics. The SEM-EDS elemental mapping of Cr in Fig. 4(c) illustrates the uniformity and continuity of Cr elements within the printed pattern. The optical image of the printed pattern on PET and nylon fabrics is shown in Fig. S4.†

Fig. 4(d) compares the Vis-NIR reflectance spectra of the printed pattern and *Scindapsus* leaves. The *Scindapsus* leaf exhibits typical spectral characteristics of green leaves: the reflection peak is located around 550 nm, called the 'green apex'; the steep inclination of reflectance appears between 680 and 780 nm, called the 'red edge'; the high reflectance of approximately 50% in the range of 780 to 1300 nm is called the 'near infrared plateau'; four absorption bands situated at 980, 1200, 1400 and 1900 nm are assigned to the combination and overtone vibration of abundant water molecules inside the leaves. Similar characteristics can be observed in the reflectance curve of the printed pattern. The 'green apex' and 'red edge' of printed pattern is caused by the absorption of Cr_2O_3, and the Cr_2O_3 particles provide a high reflectance in the range of 800 to 1300 that closely match the 'near infrared plateau' of leaves; besides, in the longer wavelength, four water absorption bands can be observed owing to the hydrophilic organic ligands capping on the surface of amorphous Cr_2O_3 particles. However, in detail, the intrinsic absorbance of Cr_2O_3 is slightly different from that of chlorophyll, which is the main contribution to the reflectance of green leaves in the visible range. On the one hand, the 'green apex' of Cr_2O_3 is blue-shifted to 535 nm; on the other hand, the slope of 'red edge' of Cr_2O_3 is much lower than that of leaves. In the near infrared range, two extra absorption bands at 1700 and 2300 nm are caused by the polyurethane layer on the fabrics. Even though, the spectral correlation coefficients[42] between the printed pattern and *Scindapsus* leaves in the range of 400–2500 nm is up to 0.9043. It is worthy to mention that the coefficients in the range of 400–680 nm and 680–1300 nm are up to 0.9203 and 0.9806 respectively.

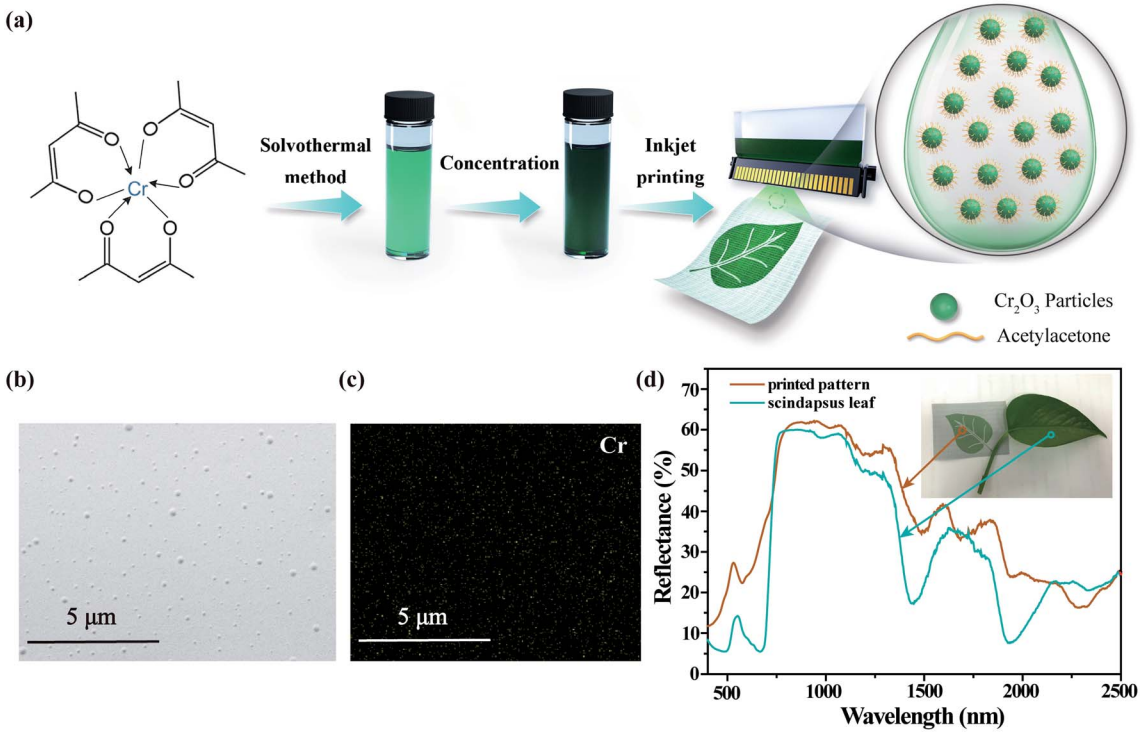

Fig. 4 (a) Schematic showing the one-step preparation and inkjet printing process of colloidal Cr_2O_3 ink. (b) SEM image and (c) SEM-EDS element mapping of Cr_2O_3 particle deposition on nylon fabrics *via* inkjet printing. (d) Vis-NIR reflectance spectra of the *Scindapsus* leaf and printed leaf-like pattern using the colloidal Cr_2O_3 ink.

Experimental section

Materials

Chromium acetylacetonate ($Cr(acac)_3$, >95%) and diethylene glycol diethyl ether (98%) were purchased from J&K Scientific. Sodium chloride standard solution (NaCl, 1 M), ethanol (>99%), poly(acrylic acid) (M_w = 450 000) and chromium oxide (99%) were purchased from Aladdin. Disperbyk-110 was purchased from BYK-Chemie® Inc. All chemicals were used as received. Nylon fabrics with a polyurethane layer were generously provided by Prof. Nanan Wang, Science and Technology on Advanced Ceramic Fibers and Composites Laboratory, National University of Defense Technology.

Preparation of Cr_2O_3 colloids

In a general procedure, 0.2 g $Cr(acac)_3$ was dissolved in 40 mL ethanol and stirred using a magnetic stirrer. After 10 min of stirring, the solution was taken into a 100 mL Teflon-lined autoclave to react under solvothermal conditions at 190 °C for 24 h. The colloids obtained were sealed and kept at room temperature. A similar procedure at different solvothermal temperatures from 180 to 220 °C with an interval of 10 °C was conducted. To elevate the throughput of this method, the amount of $Cr(acac)_3$ added was increased from 0.2 to 4.0 g.

Preparation of printing inks

The as-prepared colloids of 10 solvothermal reactions at 190 °C with 2.0 g $Cr(acac)_3$ were concentrated in a rotary evaporator. Then, 220 mL of diethylene glycol diethyl ether as a high boiling-point solvent of printing ink was added to the concentrated sample to achieve a viscosity of 5 mPa s and a surface tension of 25.8 mN m^{-1}.

Preparation of ball-milling ink

Chromium oxide, BYK-110, poly(acrylic acid), and diethylene glycol diethyl ether with a mass ratio of 4 : 0.4 : 16 : 79.6 were added to an agate jar with zirconia balls (diameters of 6 and 10 mm with a mass ratio of 1 : 1). The ball-milling process was undertaken in a planetary ball mill (Tencan Powder Technology Co., Ltd. Changsha, China) at a rotation speed of 521 rpm for 8 h. The average particle size Dx(50) of the prepared sample was 366 nm.

Inkjet printing

The ink was filtrated through a filter with a pore size of 0.45 μm before printing. Picolitre drops of the ink were ejected from a dope-on-demand inkjet system JetLab®II (MicroFab Technologies; 60 μm diameter orifice) onto the fabrics. Printing was performed at a voltage pulse of 27 V with a droplet velocity of 1.24 m s^{-1}.

Characterization

Optical absorption spectra and reflectance spectra of the samples were recorded using an ultraviolet-to-visible (UV-Vis) spectrophotometer (UV-4100). The Raman spectra of the

samples were recorded using a Raman spectrometer (Renishaw InVia) at 532 nm. The particle size was measured using a laser diffraction particle size analyser (Mastersizer 3000, Malvern Panalytical Ltd., UK). Scanning electron microscopic (SEM) images and energy-dispersive spectroscopy (EDS) mappings were recorded using a Hitachi SU8010 scanning electron microscope equipped with an EMAX Energy Dispersive Spectrometer. The X-ray diffraction patterns of samples were recorded using a powder X-ray diffractometer (Rigaku Smartlab, Cu-Kα radiation) at a scanning speed of 2° per min. Fourier transform infrared (FT-IR) spectra of the samples were also recorded (PerkinElmer Frontier). Thermogravimetric analysis (TGA) of the samples was performed using a Netzsch TGA209F1 in the temperature range of 20–1000 °C at a speed of 30 °C min^{-1} in the ambient atmosphere. The composition was determined by X-ray photoelectron spectroscopy (XPS, ESCALAB 250XI, Thermo). The dispersion stability of inks was determined using a multisample analytical centrifuge – LUMiSizer® (L.U.M. GmbH, Berlin, Germany) employing the STEP™-Technology (Space and Time resolved Extinction Profiles).

Conclusions

In conclusion, we demonstrated a one-step strategy for the fabrication of colloidal Cr_2O_3-based inkjet-printing inks by a low-temperature solvothermal method. The obtained ink remains stable under an equivalent natural sedimentation test for 2.5 years. This ink is composed of solvent and amorphous Cr_2O_3 particles capped by ethanol and acetylacetone, which is the main reason for the formation of stable homogenous colloidal dispersion. Compared with the conventional top-down fabrication process, our bottom-up strategy eliminates the risk of sedimentation, which is the major defect of the pigment printing ink. The inkjet printing of Cr_2O_3 particles was reported for the first time, and the pattern printed on fabrics is suitable for simulating solar reflection spectral characteristics of green leaves, possessing a spectral correlation coefficient up to 0.9043 in the range of 400 to 2500 nm. Many metal oxide particles with capping ligands can be synthesized by a solvothermal method.[28] Similar to our work, other metal oxides with capping ligands may exhibit good dispersion stability in certain solvents to achieve inkjet printing. Finally, although the spectral characteristics of colloidal Cr_2O_3 particles should be further tailored to achieve the same spectrum to green leaves, the inkjet printing of Cr_2O_3 provides a highly efficient and mask-free technique for camouflage patterning with flexible designability, and the idea of bottom-up ink fabrication hopefully gives a general strategy for preparing metal oxide-based pigment inks with long-term dispersion stability.

Conflicts of interest

There are no conflicts to declare.

Acknowledgements

This research is supported by National Natural Science Foundation of China 51802346, Supporting Scientific Research Project of Youth Innovation Award of National University of Defense Technology 18-QNCXJ-XXX, Key Laboratory of Science and Technology for National Defense Steadily Supports Scientific Research Project WDZC20195500505; and we acknowledge the financial support provided by National University of Defense Technology.

Notes and references

1 J. S. Gebauer, V. Mackert, S. Ognjanović and M. Winterer, *J. Colloid Interface Sci.*, 2018, **526**, 400–409.
2 S. Y. Kim, K. Kim, Y. H. Hwang, J. Park, J. Jang, Y. Nam, Y. Kang, M. Kim, H. J. Park, Z. Lee, J. Choi, Y. Kim, S. Jeong, B. S. Bae and J. U. Park, *Nanoscale*, 2016, **8**, 17113–17121.
3 T.-H. Kang, S.-W. Lee, K. Hwang, W. Shim, K.-Y. Lee, J.-A. Lim, W.-R. Yu, I.-S. Choi and H. Yi, *ACS Appl. Mater. Interfaces*, 2020, **12**, 24231–24241.
4 W. G. Whittow, 3D printing, inkjet printing and embroidery techniques for wearable antennas, *2016 10th European Conference on Antennas and Propagation (EuCAP)*, 2016.
5 M. Singh, H. M. Haverinen, P. Dhagat and G. E. Jabbour, *Adv. Mater.*, 2010, **22**, 673–685.
6 J. Suikkola, T. Björninen, M. Mosallaei, T. Kankkunen, P. Iso-Ketola, L. Ukkonen, J. Vanhala and M. Mäntysalo, *Sci. Rep.*, 2016, **6**, 25784.
7 Y. D. Kim and J. Hone, *Nature*, 2017, **544**, 167–168.
8 B. Dou, J. B. Whitaker, K. Bruening, D. T. Moore, L. M. Wheeler, J. Ryter, N. J. Breslin, J. J. Berry, S. M. Garner, F. S. Barnes, S. E. Shaheen, C. J. Tassone, K. Zhu and M. F. A. M. van Hest, *ACS Energy Lett.*, 2018, **3**, 2558–2565.
9 J. Shao, X. Chen, X. Li, H. Tian, C. Wang and B. Lu, *Sci. China: Technol. Sci.*, 2019, **62**, 175–198.
10 L. M. Cox, A. M. Martinez, A. K. Blevins, N. Sowan, Y. Ding and C. N. Bowman, *Nano Today*, 2020, **31**, 100838.
11 W. Li, Y. Wang, M. Li, L. P. Garbarini and F. G. Omenetto, *Adv. Mater.*, 2019, **31**, 1901036.
12 P. M. Theiler, F. Lütolf and R. Ferrini, *Opt. Express*, 2018, **26**, 11934–11939.
13 F. Molina-Lopez, T. Z. Gao, U. Kraft, C. Zhu, T. Öhlund, R. Pfattner, V. R. Feig, Y. Kim, S. Wang, Y. Yun and Z. Bao, *Nat. Commun.*, 2019, **10**, 2676.
14 T. Vuorinen, J. Niittynen, T. Kankkunen, T. M. Kraft and M. Mäntysalo, *Sci. Rep.*, 2016, **6**, 35289.
15 P. Calvert, *Chem. Mater.*, 2001, **13**, 3299–3305.
16 S. Sharma, S. S. Pande and P. J. R. a. Swaminathan, *RSC Adv.*, 2017, **7**, 39411–39419.
17 C. L. Nemeth, W. R. Lykins, H. Tran, M. E. H. ElSayed and T. A. Desai, *Pharm. Res.*, 2019, **36**, 89.
18 F. S. F. Brossard, V. Pecunia, A. J. Ramsay, J. P. Griffiths, M. Hugues and H. Sirringhaus, *Adv. Mater.*, 2017, **29**, 1704425.

19 Z. Pei, X. Zheng and Z. J. Li, *Nanotechnology*, 2016, **16**, 4655–4671.
20 S. Ai, H. Zheng and J. J. M. Yu, *Materials*, 2020, **13**, 1540.
21 S. Rajagopal, M. Bharaneswari, D. Nataraj, O. Y. Khyzhun and Y. Djaoued, *Mater. Res. Express*, 2016, **3**, 095019.
22 A. Lennartson, *Nat. Chem.*, 2014, **6**, 942.
23 K. Xu and H. Ye, *J. Mater. Sci.*, 2020, **55**, 12848–12863.
24 H. N. Deepak, K. S. Choudhari, S. A. Shivashankar, C. Santhosh and S. D. Kulkarni, *J. Alloys Compd.*, 2019, **785**, 747–753.
25 Y. Chen, J. Mandal, W. Li, A. Smith-Washington, C.-C. Tsai, W. Huang, S. Shrestha, N. Yu, R. P. Han and A. J. S. A. Cao, *Sci. Adv.*, 2020, **6**, eaaz5413.
26 B. Cook, Q. Liu, J. Butler, K. Smith, K. Shi, D. Ewing, M. Casper, A. Stramel, A. Elliot and J. Wu, *ACS Appl. Mater. Interfaces*, 2018, **10**, 873–879.
27 G. Wei, J. Qu, Z. Yu, Y. Li, Q. Guo and T. Qi, *Dyes Pigm.*, 2015, **113**, 487–495.
28 A. L. Willis, Z. Chen, J. He, Y. Zhu, N. J. Turro and S. O'Brien, *J. Nanomater.*, 2007, **2007**, 014858.
29 Z. Pang, J. Zhang, W. Cao, X. Kong and X. Peng, *Nat. Commun.*, 2019, **10**, 2454.
30 P. Praserthdam, J. Phungphadung and W. Tanakulrungsank, *Mater. Res. Innovations*, 2003, **7**, 118–123.
31 J. Zuo, C. Xu, B. Hou, C. Wang, Y. Xie and Y. Qian, *J. Raman Spectrosc.*, 1996, **27**, 921–923.
32 J. Mammone, S. Sharma and M. Nicol, *J. Phys. Chem.*, 1980, **84**, 3130–3134.
33 A. S. O. Gomes, N. Yaghini, A. Martinelli and E. Ahlberg, *J. Raman Spectrosc.*, 2017, **48**, 1256–1263.
34 M. Biesinger, C. Brown, J. R. Mycroft, R. D. Davidson and N. Mcintyre, *Surf. Interface Anal.*, 2004, **36**, 1550–1563.
35 S. Yu, B. Wang, Y. Pan, Z. Chen, F. Meng, S. Duan, Z. Cheng, L. Wu, M. Wang and W. Ma, *J. Clean. Prod.*, 2018, **176**, 636–644.
36 S. P. Narayanan, P. Thakur, A. P. Balan, A. A. Abraham, F. Mathew, M. Yeddala, T. Subair, C. Tiwary, S. Thomas, T. N. Narayanan, P. M. Ajayan and M. M. R. Anantharaman, *Phys. Status Solidi RRL*, 2019, **13**, 1900025.
37 H. Kamack, *Anal. Chem.*, 1951, **23**, 844–850.
38 T. Detloff, T. Sobisch and D. Lerche, *Part. Part. Syst. Charact.*, 2006, **23**, 184–187.
39 D. Lerche and T. Sobisch, *Powder Technol.*, 2007, **174**, 46–49.
40 W. Hoffmann and K. Schrader, *Int. J. Food Sci. Technol.*, 2015, **50**, 950–957.
41 T. Detloff, T. Sobisch and D. Lerche, *Dispersion Letters Technical*, 2013, 1–4.
42 A. Hu, M. Li, L. Zhang, C. Wang and S. Fu, *RSC Adv.*, 2019, **9**, 41438–41446.